Available online at www.sciencedirect.com

SciVerse ScienceDirect

Solar Energy 86 (2012) 941–950

SOLAR ENERGY

www.elsevier.com/locate/solener

Determination of the angular parameters in the general altitude–azimuth tracking angle formulas for a heliostat with a mirror-pivot offset based on experimental tracking data

Minghuan Guo, Zhifeng Wang *, Jianhan Zhang, Feihu Sun, Xiliang Zhang

Key Laboratory of Solar Thermal Energy and Photovoltaic System of Chinese Academy of Sciences, Institute of Electrical Engineering, Beijing 100190, China

Received 16 September 2011; received in revised form 23 December 2011; accepted 24 December 2011
Available online 19 January 2012

Communicated by: Associate Editor L. Vant-Hull

Abstract

A set of general altitude–azimuth tracking angle formulas for a heliostat with a mirror-pivot offset and other geometrical errors were developed previously. The angular parameters with respect to the geometrical errors are the tilt angle, ψ_t, and the tilt azimuth angle, ψ_a, of the azimuth axis, the bias angle, τ_1, of the altitude axis from the orthogonal to the azimuth axis, and the canting angle, μ, of the mirror surface plane relative to the altitude axis. In view of the importance the zero angle position errors of the two rotational axes (α_0 is for the zero angle position error of the altitude axis and γ_0 for the zero angle position error of the azimuth axis), the original general tracking angle formulae have been slightly modified by replacing the tracking angles in the original tracking formulas with the difference between the nominal tracking angles and the zero angle position errors. The six angular parameters (ψ_a, ψ_t, γ_0, τ_1, α_0, μ) for a specific altitude–azimuth tracking heliostat could be determined from experimental tracking data using a least squares fit and the classical Hartley-Meyer solution algorithm. The least squares model is used on data for a specially designed heliostat model with two sets of laser beam tracking test data to show the effectiveness of the least squares model and the Hartley-Meyer algorithm.

Keywords: Heliostat; Altitude–azimuth tracking; Angular parameters; Least squares

1. Introduction

The solar field of a solar tower system consists of an array of heliostats on the ground with each heliostat tracking the sun on two axes to continuously reflect the solar radiation onto the tower-top receiver. Accurate dual-axis sun tracking is the key feature of a heliostat and is very important for the optical performance. Various dual-axis tracking modes have been given in the literature (Lipps and Vant-Hull, 1978), such as altitude–azimuth, radial-pitch-roll, azimuth-pitch-roll, polar and receiver oriented. Guo et al. (2010) gave an overview of dual-axis tracking modes and the geometric nature of these tracking modes. Given the same geometric position of the aim point, the sun and the mirror pivot (intersection of the two rotational axes), all these tracking modes should have the same mirror normal at the mirror surface centre to guide the reflected sun beam from the mirror surface to the aim point. Of these dual-axis tracking modes, the altitude–azimuth tracking mode is the most common and popular for solar collectors. With the altitude–azimuth tracking mode, the azimuth axis is the primary axis and is fixed to the ground plane, pointing towards the zenith. The altitude axis is the secondary axis and is rotating orthogonal to the azimuth axis.

Guo et al. (2010) gave high precision tracking formulas to calibrate the effect of the mirror–pivot offset for a standard receiver oriented heliostat assuming that the

* Corresponding author. Tel.: +86 10 62520684; fax: +86 10 62587946.
E-mail address: zhifeng@vip.sina.com (Z. Wang).

0038-092X/$ - see front matter © 2011 Elsevier Ltd. All rights reserved.
doi:10.1016/j.solener.2011.12.025

rotational axes were orthogonal and the secondary axis was parallel to the mirror surface plane. Guo et al. (2011) further linked the altitude–azimuth tracking mode with the receiver oriented tracking mode and studied the geometric errors of an altitude–azimuth tracking heliostat due to mechanism imperfections with the general altitude–azimuth tracking angle formulas for a heliostat with both a mirror-pivot offset and other angular geometric errors. In these tracking angle formulas, the altitude tracking angle is α, and the azimuth tracking angle is γ. The mirror-pivot offset, H_z, is defined as the distance from the mirror pivot to the mirror surface centre (the orthogonal projection of the heliostat pivot on the mirror surface plane). The angular errors are the heliostat pedestal tilt from the vertical, the non-orthogonality of the two rotational axes and the non-parallel degree between the mirror surface plane and the altitude axis. The four angular parameters in the altitude–azimuth tracking formulas are the tilt angle, ψ_t, and the tilt azimuth angle, ψ_a, of the azimuth axis, the dual-axis non-orthogonal angle, τ_1 (bias angle of the altitude axis from the orthogonal to the azimuth axis), and the canting angle, μ, of the mirror surface plane relative to the altitude axis.

For the geometry in Fig. 1, point **O** stands for the heliostat pivot with vectors **OT**, **ON**,**OS** being the vectors pointing to the aim point **T**, the mirror-surface-center normal and the solar vector. In Fig. 1, $\mathbf{\Pi}_1$ is the dual-axis plane containing the azimuth axis and the altitude axis, $\mathbf{\Pi}_2$ is the plane determined by the altitude axis and the mirror surface center **M**, θ^* is the sun beam incident angle at **M**, $\mathbf{O_T}$ is the vertical projection of **T** on the horizontal ground plane, and $\mathbf{O_H}$ is the intersection of the azimuth axis with the horizontal ground plane. $\mathbf{\Pi}_2$ is also the E_1–E_2 plane of the local left-hand Cartesian coordinate system [**O**; E_1–E_2–E_3]. When $\psi_t = 0°$, $\tau_1 = 0°$, $\mu = 0°$, $\gamma = 0°$ and $\alpha = 0°$, the heliostat is in the vertical position with the mirror-surface-center normal $\vec{n}$ horizontal and pointing exactly north, i.e. $\vec{n} = (1, 0, 0)$ in a left-handed Cartesian coordinate system [**O**; North-East-Height].

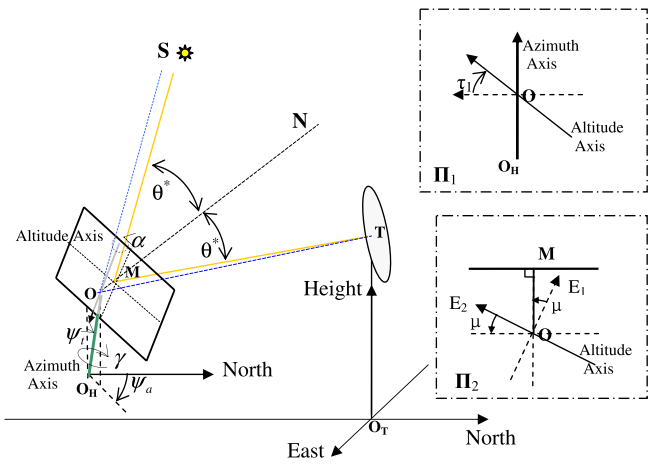

Fig. 1. Altitude–azimuth tracking geometry and definitions of the angular parameters for a heliostat with a mirror-pivot offset. The left side is the 3D plot of the heliostat tracking geometry, while the right side has 2D plots of plane $\mathbf{\Pi}_1$ and $\mathbf{\Pi}_2$ marked by dashed and dotted lines. $\mathbf{\Pi}_1$ is the dual-axis plane containing the azimuth axis and the altitude axis while $\mathbf{\Pi}_2$ is the plane determined by the altitude axis and the mirror surface center **M**. $\mathbf{\Pi}_1$ and $\mathbf{\Pi}_2$ show the dual-axis non-orthogonal angle, τ_1, and canting angle, μ. $\mathbf{\Pi}_2$ is also the E_1–E_2 plane of the local left-handed Cartesian coordinate system [**O**; E_1–E_2–E_3]. γ and α are the azimuth and altitude tracking angles of the altitude–azimuth tracking heliostat. The left-handed rotational direction is positive for the azimuth axis, while the right-handed rotational direction is positive for the altitude axis. ψ_t and ψ_a are the tilt angles for the azimuth axis from the vertical direction. τ_1 is the bias angle of the altitude axis from the orthogonal to the azimuth axis. μ is the canting angle of the mirror surface plane relative to the altitude axis.

The encoder reference errors are not explicitly expressed in the altitude–azimuth tracking angle formulas since the encoder reference errors can be directly added to the altitude tracking angle, α, and the azimuth tracking angle, γ.

The encoder reference errors directly affect the zero angle positions of the two rotational axes relative to their initial axis limit sensors, so the encoder reference errors can be merged into the zero angle positions of the two rotational axes. If using $\alpha = \alpha' - \alpha_0$ and $\gamma = \gamma' - \gamma_0$, then the altitude–azimuth tracking angle formulas turn into the extensional tracking angle formulas for an altitude–azimuth tracking heliostat. Here, α_0 is the angular difference between the real zero angle position and the nominal zero angle position of the altitude axis, γ_0 is the angular difference between the real zero angle position and the nominal zero angle position of the azimuth axis, α' is the nominal altitude tracking angle, and γ' is the nominal azimuth tracking angle. The tracking angle α for the nominal zero angle position of the altitude axis is $-\alpha_0$ and the tracking angle γ for the nominal zero angle position of the azimuth axis is $-\gamma_0$.

The geometric tracking parameters in the extensional altitude–azimuth tracking angle formulas must be determined in advance when those tracking angle formulas are applied to a real heliostat. The distance can be easily and accurately measured using modern high-tech surveying instruments. The tracking accuracy of a heliostat over the target plane is less sensitive to distance metric errors than to angular parameter errors. Thus, the task is to find the six angular tracking parameters, (ψ_a, ψ_t, γ_0, τ_1, α_0, μ) for a real altitude–azimuth tracking heliostat.

Open-loop tracking control is usually used with heliostats in solar tower systems, with auxiliary equipment, such as the beam characterization system (BCS) used at Solar One (King, 1982; Mavis, 1988; Strachan, 1993), used to calibrate the heliostat tracking errors on the experimental target board. BCS includes a Lambertian target, a B/W CCD camera, reference radiometers, and neutral density filters, as well as the image acquisition and data processing software.

Stone and Jones (1999) pointed out that the three dominant geometric errors in a heliostat in the solar tower power plant of Solar Two were the azimuth axis tilt, the mirror canting error, and encoder reference errors. They graphically analyzed the effects of these geometric errors on the heliostat tracking accuracy and gave two strategies

to improve the heliostat tracking accuracy, including a bias strategy for the encoder references and a virtual move strategy for the heliostat position in the solar field. Jones and Stone (1999) used BCS to further compare the tracking error correction results of the Bias strategy, the Move strategy and a newly developed Error-correction model. Jones and Stone favored the Error-correction model which was based on the altitude–azimuth tracking geometry with geometric errors, but the Error-correction model was not described in the report (Jones and Stone, 1999) and was not actually used in Solar Two at that time. A simplified, automatic heliostat positioning offset correction control system developed at PSA in Spain was also based on a common CCD camera, a target board near the receiver aperture, and a simple tracking error correction model (Berenguel et al., 2004).

BCS can be used to easily identify the image centres on the heliostat target plane and the measured tracking data can be easily used to evaluate the tracking performance or to calibrate the heliostat tracking errors.

This paper describes a nonlinear least squares model to determine the six angular parameters in the extensional altitude–azimuth tracking formulas, with a classical, effective algorithm to solve this least squares model to fit the experimental tracking data. The least squares model is then used to determine the angular tracking parameters of a test heliostat model with indoor laser beam tracking data to verify the effectiveness of the least squares model.

2. Intersection of the reflected mirror-surface-centre ray with the target plane

The intersection of the reflected mirror-surface-centre ray with the target plane is determined based on the current altitude tracking angle, azimuth tracking angle, and sun position vector. The intersection point of the reflected central ray is expressed by U–V coordinates on the local target plane.

2.1. Intersection of the reflected central ray with the target plane

The geometry for the intersection of the reflected mirror-surface-centre ray with the heliostat target plane with a mirror-pivot offset is drawn in Fig. 2. In Fig. 2, [**O**; North-East-Height] is a left-handed Cartesian coordinate system where origin **O** is the mirror pivot (intersection of the two rotational axes), **M** is the mirror-surface centre defined as the orthogonal projection of **O** on the mirror surface plane, $\vec{n}$ is the unit vector for the mirror centre normal **ON**; $\mathbf{T}_0$ is the origin of the left-handed target coordinate system $[\mathbf{T}_0;\ \vec{\xi}-\vec{\eta}-\vec{n}_t]$, $\vec{n}_t$ is the unit normal of the target plane, $\vec{\eta}$ points downward and $\vec{\xi}$ is the horizontal. $\vec{s}$ is the unit solar vector and θ^* is the incident angle of a solar ray on the mirror surface centre. **T** and **T′** on the target plane are the computed intersection and the observed

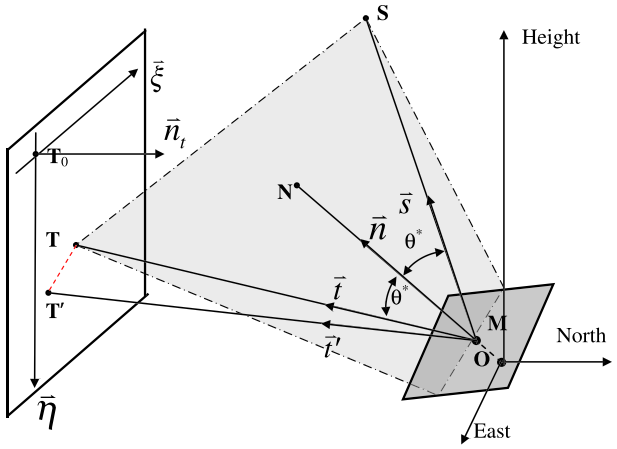

Fig. 2. Intersection geometry of the reflected mirror-surface-centre ray with the target plane for a heliostat with a mirror-pivot offset. **M** is the mirror-surface centre while points **T** and **T′** are the computed intersection and the observed intersection of the reflected central ray with the target plane. $\mathbf{T}_0$ is the origin of the target plane, $\vec{n}_t$ is normal to the target plane, and $\vec{n}$ is the unit normal at the mirror surface centre **M**.

intersection of the reflected solar ray from **M**. $\vec{t}$ is the unit vector for vector **MT** and $\vec{t}'$ is the unit vector for **MT′**.

In the target coordinate system $[\mathbf{T}_0;\ \vec{\xi}-\vec{\eta}-\vec{n}_t]$, the coordinates of **T** are $(u,v,0)$ and of **T′** are $(u',v',0)$, i.e. $\mathbf{T}_0\mathbf{T} = \mathrm{u}\,\vec{\xi} + \mathrm{v}\,\vec{\eta}$ and $\mathbf{T}_0\mathbf{T}' = u'\,\vec{\xi} + v'\,\vec{\eta}$.

In coordinate system [**O**; North-East-Height], $\vec{n} = (n_1, n_2, n_3)$, vector $\mathbf{OM} = H_z\,\vec{n}$, the mirror-pivot offset is $\|\mathbf{OM}\| = H_z$, $\vec{t}_0 = \mathbf{OT}_0 = (t_1^0, t_2^0, t_3^0)$, $\vec{n}_t = (\cos\phi_t\cos\phi_a, \cos\phi_t\sin\phi_a, \sin\phi_t)$, and ϕ_a and ϕ_t are the azimuth angle and the altitude angle of $\vec{n}_t$, respectively. For the current solar altitude angle, α_s, and the solar azimuth angle, γ_s (in the north-to-east direction), the solar vector is expressed as

$$\vec{s} = (s_1, s_2, s_3) = (\cos\alpha_s\cos\gamma_s, \cos\alpha_s\sin\gamma_s, \sin\alpha_s) \tag{1}$$

2.2. Computation of the mirror centre normal from tracking angles

According to Guo et al. (2011) and as shown in Fig. 1, the mirror-surface-center normal $\vec{n} = (\cos\mu, \sin\mu, 0)$ in the local coordinate system [**O**; E_1–E_2–E_3] can be transformed into $\vec{n} = (\mathrm{n}_1, \mathrm{n}_2, \mathrm{n}_3)$ in coordinate system [**O**; North-East-Height] through eight successive rotational transformation matrices. Equivalently, the E_1 axis can be moved to the North axis with the same eight rotational transformations applied in order, using the left-hand rule from the local coordinate system [**O**; E_1–E_2–E_3] to coordinate system [**O**; North-East-Height]. These rotational transformation matrices are:

$$\mathrm{B}_1 = \mathrm{B}_1(3,\ \psi_a) = \begin{bmatrix} \cos\psi_a & \sin\psi_a & 0 \\ -\sin\psi_a & \cos\psi_a & 0 \\ 0 & 0 & 1 \end{bmatrix} \tag{2}$$

$$\mathrm{B}_2 = \mathrm{B}_2(2,\ \psi_t) = \begin{bmatrix} \cos\psi_t & 0 & -\sin\psi_t \\ 0 & 1 & 0 \\ \sin\psi_t & 0 & \cos\psi_t \end{bmatrix} \tag{3}$$

$$\mathrm{B}_3 = \mathrm{B}_3(3,\ -\psi_a) = \begin{bmatrix} \cos\psi_a & -\sin\psi_a & 0 \\ \sin\psi_a & \cos\psi_a & 0 \\ 0 & 0 & 1 \end{bmatrix} \tag{4}$$

$$\mathrm{B}_{4a} = \mathrm{B}_{4a}(3,\ -\gamma_0) = \begin{bmatrix} \cos\gamma_0 & -\sin\gamma_0 & 0 \\ \sin\gamma_0 & \cos\gamma_0 & 0 \\ 0 & 0 & 1 \end{bmatrix} \tag{5}$$

$$\mathrm{B}_{4b} = \mathrm{B}_{4b}(3,\ \gamma') = \begin{bmatrix} \cos\gamma' & \sin\gamma' & 0 \\ -\sin\gamma' & \cos\gamma' & 0 \\ 0 & 0 & 1 \end{bmatrix} \tag{6}$$

$$\mathrm{B}_5 = \mathrm{B}_5(1,\ \tau_1) = \begin{bmatrix} 1 & 0 & 0 \\ 0 & \cos\tau_1 & \sin\tau_1 \\ 0 & -\sin\tau_1 & \cos\tau_1 \end{bmatrix} \tag{7}$$

$$\mathrm{B}_{6a} = \mathrm{B}_{6a}(2,\ \alpha_0) = \begin{bmatrix} \cos\alpha_0 & 0 & -\sin\alpha_0 \\ 0 & 1 & 0 \\ \sin\alpha_0 & 0 & \cos\alpha_0 \end{bmatrix} \tag{8}$$

$$\mathrm{B}_{6b} = \mathrm{B}_{6b}(2,\ -\alpha') = \begin{bmatrix} \cos\alpha' & 0 & \sin\alpha' \\ 0 & 1 & 0 \\ -\sin\alpha' & 0 & \cos\alpha' \end{bmatrix}. \tag{9}$$

$\mathrm{B}_1(3,\ \psi_a)$ is the initial coordinate system ([**O**; North-East-Height]) to a new coordinate system position around the 3rd axis through the angle ψ_a in the left-hand direction. $\mathrm{B}_2(2,\ \psi_t)$ then further rotates the result of the $\mathrm{B}_1(3,\ \psi_a)$ rotation to the next coordinate system position around the 2nd axis through the angle ψ_t in the positive left-hand direction. $\mathrm{B}_3(3,\ -\psi_a)$, $\mathrm{B}_{4a}(3,\ -\gamma_0)$, $\mathrm{B}_{4b}(3,\ \gamma')$, $\mathrm{B}_5(1,\ \tau_1)$, $\mathrm{B}_{6a}(2,\ \alpha_0)$ and $\mathrm{B}_{6b}(2,\ -\alpha')$ are similar rotations where '$-\psi_a$' in B_3, '$-\gamma_0$' in B_{4a} and '$-\alpha'$' in B_{6b} stand for the rotation angles ψ_a, γ_0 and α' in the right-hand direction.

The mirror centre normal $\vec{n}$ in coordinate system [**O**; North-East-Height] is:

$$\begin{aligned} \vec{n} &= (n_1, n_2, n_3) \\ &= (\cos\mu, \sin\mu, 0)\ (\mathrm{B}_{6b}\ \mathrm{B}_{6a}\mathrm{B}_5\mathrm{B}_{4b}\ \mathrm{B}_{4a}\mathrm{B}_3\mathrm{B}_2\mathrm{B}_1). \end{aligned} \tag{10}$$

2.3. U–V coordinates of the intersection of the reflected mirror-surface-centre ray on the target plane

From Eqs. (1)–(10) and Fig. 2, the unit vector $\vec{t}$ of the reflected mirror centre ray **MT** can be computed as

$$\cos(\theta^*) = \vec{s} \bullet \vec{n} \tag{11}$$

$$\vec{t} = (t_1, t_2, t_3) = -\vec{s} + 2\vec{n}\cos(\theta^*) \tag{12}$$

Vector **OT** can be computed as

$$\lambda_p = \frac{\left(\vec{n}_t \bullet \vec{t}_0\right) - H_z\left(\vec{n}_t \bullet \vec{n}\right)}{\left(\vec{n}_t \bullet \vec{t}\right)} \tag{13}$$

$$\begin{aligned} \mathbf{OT} &= \mathbf{OM} + \mathbf{MT} = H_z\vec{n} + \lambda_p\vec{t} \\ &= H_z\vec{n} + \frac{\left(\vec{n}_t \bullet \vec{t}_0\right)\vec{t} - H_z\left(\vec{n}_t \bullet \vec{n}\right)\vec{t}}{\left(\vec{n}_t \bullet \vec{t}\right)} \end{aligned} \tag{14}$$

Thus,

$$\begin{aligned} \mathbf{T}_0\mathbf{T} &= \mathbf{OT} - \mathbf{OT}_0 \\ &= H_z\vec{n} + \frac{\left(\vec{n}_t \bullet \vec{t}_0\right)\vec{t} - H_z\left(\vec{n}_t \bullet \vec{n}\right)\vec{t}}{\left(\vec{n}_t \bullet \vec{t}\right)} - \vec{t}_0 \end{aligned} \tag{15}$$

Using $\mathbf{T}_0\mathbf{T} = \mathrm{u}\,\vec{\xi} + \mathrm{v}\,\vec{\eta}$, the U–V coordinates of **T** are

$$u = \mathbf{T}_0\mathbf{T} \bullet \vec{\xi} \tag{16}$$

$$v = \mathbf{T}_0\mathbf{T} \bullet \vec{\eta} \tag{17}$$

3. Least squares model and solution algorithm to determine the angular tracking parameters

A least squares model was used to determine the angular parameters (ψ_a, ψ_t, γ_0, τ_1, α_0, μ) in the general altitude–azimuth tracking angle formulas for a heliostat with a mirror-pivot offset. A classical algorithm is used to obtain the least squares solution.

3.1. Least squares model

Determination of the angular tracking parameters (ψ_a, ψ_t, γ_0, τ_1, α_0, μ) in the general altitude–azimuth tracking angle formulas requires q ($q \geqslant J = 6$) independent altitude–azimuth tracking tests to obtain a least squares fit. The six angular parameters are given in the least squares model as:

$$\vec{x} = (x_1, x_2, x_3, x_4, x_5, x_6) = (\psi_a, \psi_t, \gamma_0, \tau_1, \alpha_0, \mu). \tag{18}$$

The experimental data points obtained in the heliostat tracking tests are

- solar position angles: $\alpha_{s,i}$ and $\gamma_{s,i}$, $i = 1, 2, \ldots, q$,
- nominal altitude–azimuth tracking angles: γ'_i and α'_i, $i = 1, 2, \ldots, q$.
- observed U–V coordinates of $\mathbf{T}'$: (u'_i, v'_i), $i = 1, 2, \ldots, q$.

The unit solar vectors $\vec{s}_i = (s_{1,i}, s_{2,i}, s_{3,i})$ with respect to $\alpha_{s,i}$ and $\gamma_{s,i}$ are computed using Eq. (1). The mirror centre normals $\vec{n}_i = (n_{1,i}, n_{2,i}, n_{3,i})$ are computed using Eqs. (2)–(10). The unit vectors of the reflected mirror centre ray, $\vec{t}_i = (t_{1,i}, t_{2,i}, t_{3,i})$, are computed using Eqs. (11) and (12). $\vec{n}_i$ and $\vec{t}_i$ are functions of vector $\vec{x} = (x_1, x_2, x_3, x_4, x_5, x_6)$, i.e. $\vec{n}_i = \vec{n}_i(\vec{x})$, $\vec{t}_i = \vec{t}_i(\vec{x})$, $i = 1, 2, \ldots, q$.

Once $\vec{n}_i$ and $\vec{t}_i$ are known, the U–V coordinates of each intersection of the reflected mirror-surface-centre ray with the target plane can be computed using Eqs. (15)–(17). The computed U–V coordinates are given by $u_i(\vec{x})$ and $v_i(\vec{x})$. According to Eq. (15), both $u_i(\vec{x})$ and $v_i(\vec{x})$ are functions of $\vec{n}_i = \vec{n}_i(\vec{x})$ and $\vec{t}_i = \vec{t}_i(\vec{x})$.

A nonlinear least squares model was then used to determine the six angular tracking parameters with the error functions, $f_i(\vec{x})$, and the objective function, $S(\vec{x})$, formulated as:

$$f_i(\vec{x}) = \sqrt{(u_i(\vec{x}) - u_i')^2 + (v_i(\vec{x}) - v_i')^2}, \quad i = 1, 2, \ldots, q \tag{19}$$

$$S(\vec{x}) = \sum_{i=1}^{q} f_i^2(\vec{x}) \tag{20}$$

3.2. Jacobian matrix

The q error functions $f_i(\vec{x})$ are arranged in vector form as

$$\vec{f}(\vec{x}) = \left(f_1(\vec{x}), f_2(\vec{x}), f_3(\vec{x}), \ldots, f_q(\vec{x})\right)^T \tag{21}$$

The Jacobian matrix of $\vec{f}(\vec{x})$ is defined as

$$\widetilde{J}(\vec{x}) = \begin{pmatrix} \frac{\partial f_1(\vec{x})}{\partial x_1} & \cdots & \frac{\partial f_1(\vec{x})}{\partial x_J} \\ \vdots & \ddots & \vdots \\ \frac{\partial f_q(\vec{x})}{\partial x_1} & \cdots & \frac{\partial f_I(\vec{x})}{\partial x_J} \end{pmatrix}. \tag{22}$$

The computing of $\widetilde{J}(\vec{x})$ is done layer by layer as:

$$\begin{cases} \frac{\partial f_i(\vec{x})}{\partial x_j} = \frac{\left(u_i(\vec{x}) - u_i'\right)}{f_i(\vec{x})} \frac{\partial u_i(\vec{x})}{\partial x_j} + \frac{\left(v_i(\vec{x}) - v_i'\right)}{f_i(\vec{x})} \frac{\partial v_i(\vec{x})}{\partial x_j} \\ i = 1, 2, \ldots, q; \; j = 1, 2, \ldots, J \end{cases} \tag{23}$$

$$\frac{\partial u_i(\vec{x})}{\partial x_j} = \frac{\partial (\mathbf{T_0 T})_i}{\partial x_j} \bullet \vec{\xi} \tag{24}$$

$$\frac{\partial v_i(\vec{x})}{\partial x_j} = \frac{\partial (\mathbf{T_0 T})_i}{\partial x_j} \bullet \vec{\eta} \tag{25}$$

$$\begin{aligned} \frac{\partial (\mathbf{T_0 T})_i}{\partial x_j} &= \frac{\partial \left(H_z \vec{n}_i + \frac{\left(\vec{n}_t \bullet \vec{t}_0\right)\vec{t}_i - H_z\left(\vec{n}_t \bullet \vec{n}_i\right)\vec{t}_i}{\left(\vec{n}_t \bullet \vec{t}_i\right)} - \vec{t}_0 \right)}{\partial x_j} \\ &= H_z \frac{\partial \vec{n}_i}{\partial x_j} + \frac{\left(\vec{n}_t \bullet \vec{t}_0\right)\left[\frac{\partial \vec{t}_i}{\partial x_j}\left(\vec{n}_t \bullet \vec{t}_i\right) - \vec{t}_i\left(\vec{n}_t \bullet \frac{\partial \vec{t}_i}{\partial x_j}\right)\right]}{\left(\vec{n}_t \bullet \vec{t}_i\right)^2} \\ &\quad + \frac{H_z\left[\left(\vec{n}_t \bullet \vec{n}_i\right)\left(\vec{n}_t \bullet \frac{\partial \vec{t}_i}{\partial x_j}\right)\vec{t}_i - \left(\vec{n}_t \bullet \vec{t}_i\right)\left(\left(\vec{n}_t \bullet \frac{\partial \vec{n}_i}{\partial x_j}\right)\vec{t}_i + \left(\vec{n}_t \bullet \vec{n}_i\right)\frac{\partial \vec{t}_i}{\partial x_j}\right)\right]}{\left(\vec{n}_t \bullet \vec{t}_i\right)^2} \end{aligned} \tag{26}$$

$$\frac{\partial \vec{t}_i}{\partial x_j} = 2\left(\vec{n}_i \bullet \vec{s}_i\right)\frac{\partial \vec{n}_i}{\partial x_j} + 2\vec{n}_i\left(\frac{\partial \vec{n}_i}{\partial x_j} \bullet \vec{s}_i\right) \tag{27}$$

$$\begin{aligned} \frac{\partial \vec{n}_i}{\partial x_1} &= \frac{\partial \vec{n}_i}{\partial \psi_a} = (\cos\mu, \sin\mu, 0)\left(B_{6b,i}B_{6a}B_5B_{4b,i}B_{4a}\right) \\ &\quad \times \left(\frac{\partial B_3}{\partial \psi_a}B_2B_1 + B_3B_2\frac{\partial B_1}{\partial \psi_a}\right) \end{aligned} \tag{28}$$

$$\begin{aligned} \frac{\partial \vec{n}_i}{\partial x_2} &= \frac{\partial \vec{n}_i}{\partial \psi_t} \\ &= (\cos\mu, \sin\mu, 0)\left(B_{6b,i}B_{6a}B_5B_{4b,i}B_{4a}B_3\frac{\partial B_2}{\partial \psi_t}B_1\right) \end{aligned} \tag{29}$$

$$\begin{aligned} \frac{\partial \vec{n}_i}{\partial x_3} &= \frac{\partial \vec{n}_i}{\partial \gamma_0} = (\cos\mu, \sin\mu, 0) \\ &\quad \times \left(B_{6b,i}B_{6a}B_5B_{4b,i}\frac{\partial B_{4a}}{\partial \gamma_0}B_3B_2B_1\right) \end{aligned} \tag{30}$$

$$\frac{\partial \vec{n}_i}{\partial x_4} = \frac{\partial \vec{n}_i}{\partial \tau_1} = (\cos\mu, \sin\mu, 0)\left(B_{6b,i}B_{6a}\frac{\partial B_5}{\partial \tau_1}B_{4b,i}B_{4a}B_3B_2B_1\right) \tag{31}$$

$$\frac{\partial \vec{n}_i}{\partial x_5} = \frac{\partial \vec{n}_i}{\partial \alpha_0} = (\cos\mu, \sin\mu, 0)\left(B_{6b,i}\frac{\partial B_{6a}}{\partial \alpha_0}B_5B_{4b,i}B_{4a}B_3B_2B_1\right) \tag{32}$$

$$\frac{\partial \vec{n}_i}{\partial x_6} = \frac{\partial \vec{n}_i}{\partial \mu} = (-\sin\mu, \cos\mu, 0)\left(B_{6b,i}B_{6a}B_5B_{4b,i}B_{4a}B_3B_2B_1\right) \tag{33}$$

Eqs. (23)–(33) are all required to compute $\widetilde{J}(\vec{x})$ defined in Eq. (22) in terms of $\vec{x}$.

The gradient of the objective function, $S(\vec{x})$, is formulated as

$$gradS(\vec{x}) = \nabla S(\vec{x}) = 2\widetilde{J}^T(\vec{x})\vec{f}(\vec{x}). \tag{34}$$

The root of the mean square of the error functions, $f_i(\vec{x})$, is

$$rms\_error(\vec{x}) = \sqrt{\sum_{i=1}^{q} f_i^2(\vec{x})/q} = \sqrt{S(\vec{x})/q}. \tag{35}$$

The units for the six angular elements in $\vec{x}$ in the least squares model are radians.

3.3. Hartley-Meyer algorithm for solving the least squares model

The Hartley-Meyer algorithm is a modified Gauss–Newton algorithm for solving the nonlinear least squares equations. This is a simple, practical algorithm to determine the fixed angular parameters in the general altitude–azimuth tracking angle formulas. The Hartley-Meyer algorithm is described in detail by Zhang et al. (1989) and given here for convenience.

Given the proper positive precision control parameters ε_1 and ε_2, trust region parameter β_b, and an initial value of $\vec{x}$, i.e. $\vec{x}_0 = (x_1^0, x_2^0, x_3^0, x_4^0, x_5^0, x_6^0) = \left(\psi_a^0, \psi_t^0, \gamma_0^0, \tau_1^0, \alpha_0^0, \mu^0\right)$, the iterative Hartley-Meyer algorithm can then be formulated as:

Step 1: $k = 0$.
Step 2: $\vec{f}_k = \vec{f}(\vec{x}_k)$ using Eqs. (19) and (21).
Step 3: $\widetilde{J}_k = \widetilde{J}(\vec{x}_k)$ using Eq. (22).
Step 4: $S(\vec{x}_k) = \left(\vec{f}_k\right)^T\vec{f}_k$, $\vec{g}_k = \widetilde{J}_k^T\vec{f}_k$.

Step 5: $\Delta\vec{x}_k = -\left(\widetilde{J}_k^T\widetilde{J}_k\right)^{-1}\vec{g}_k$.
Step 6: $\beta_a = 1.0$.
Step 7: $\vec{f}'_k = \vec{f}(\vec{x}_k + \beta_a\Delta\vec{x}_k)$ using Eqs. (19) and (21).
Step 8: $S'(\vec{x}_k) = (\vec{f}'_k)^T\vec{f}'_k$.
Step 9: if $S'(\vec{x}_k) \geqslant S(\vec{x}_k) + 2\beta_a\beta_b(\Delta\vec{x}_k)^T\vec{g}_k$, then {$\beta_a = \beta_a/2$, go to Step 7}.
Step 10: $\vec{x}_{k+1} = \vec{x}_k + \beta_a\Delta\vec{x}_k$, $\nabla S(\vec{x}_{k+1}) = 2\widetilde{J}^T(\vec{x}_{k+1})\vec{f}(\vec{x}_{k+1})$.
Step 11: if $|\beta_a\Delta\vec{x}_k| < \varepsilon_1$ or $|\nabla S(\vec{x}_{k+1})| < \varepsilon_2$, then {$k = k+1$, go to End}.
Step 12: $k = k+1$.
Step 13: if $k < 1000$, then go to Step 2End: stop iterating, get the solution of the least squares model, $\vec{x}^* = \vec{x}_k$ and also the minimum value of the objective function, $S(\vec{x}^*)$.

Here, k is the counter for the iteration loop to update $\vec{x}$, while ε_1 and ε_2 are the error limits input to the iteration process. Generally, β_b=10^{-5}. The upper limit of 1000 is given in case of non-convergence.

The flow diagram for the Hartley-Meyer algorithm is given in Fig. 3.

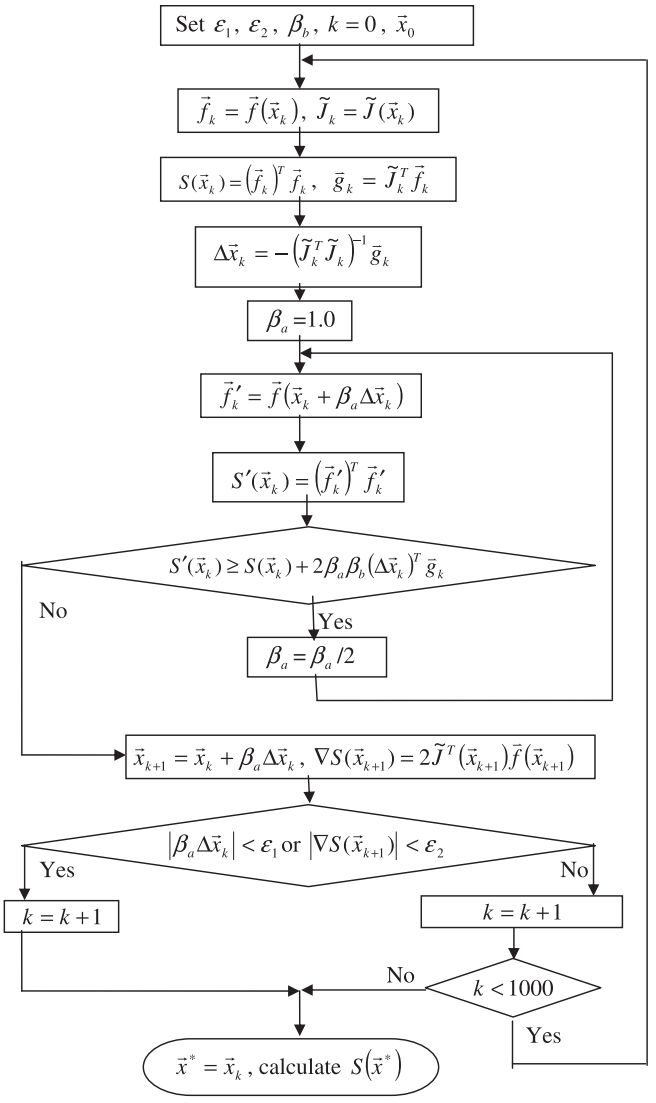

Fig. 3. Flow chart of the Hartley-Meyer algorithm for solving the least squares model.

4. Determination of the angular parameters of a laser-beam-tracking heliostat mode from tracking test data

The validity of the least squares model and the Hartley-Meyer solution algorithm was evaluated by determining the six angular tracking parameters of a specially designed heliostat mode.

4.1. Laser beam tracking test setup for the altitude–azimuth tracking heliostat model

A specially designed heliostat model with altitude–azimuth tracking was built on the platform of a three-dimensional coordinate measuring machine (3D CMM) with a movable vertical laser. The test setup and the laser beam altitude–azimuth tracking tests were described by Guo et al. (2011). The laser beam altitude–azimuth tracking heliostat model constructed on the 3D CMM platform is shown in Fig. 4a. The azimuth and the altitude motors were both 24V DC torque motors with no reduction gears. The physical resolution of the encoders was 5000 lines per revolution, i.e. 360°/5000 = 0.072°. The angular positioning accuracies of the two drive motors were further enhanced by the fourfold frequency multiplication technique applied to the drive controllers. The interface software for the two servo drive controllers always truncated the input tracking angles to an accuracy of one decimal (i.e. 0.1°). Fig. 4b shows a rectangular box placed on the floor on the south side of the CMM platform with a sheet of 500 mm × 350 mm coordinate paper used as a tracking target plane attached to the front wall of the cabinet which is exactly horizontal and north facing. This coordinate paper gives a two-dimensional target coordinate system [$\mathbf{T}_0$; $\vec{\xi} - \vec{\eta}$], where the origin $\mathbf{T}_0$ is at the left-top corner of the grid area on the target paper, the horizontal $\vec{\xi}$ axis coincides with the west direction and the vertical $\vec{\eta}$ axis is in the negative height direction.

In the coordinate system [**O**; North-East-Height], the origin **O** is the heliostat pivot, the laser beam vector (which models the solar vector) $\vec{s} = (0, 0, 1)$, $\mathbf{T}_0 = 0.001\times(-2593.9, 348.76, 763.79)$, and $\|\mathbf{OT}_0\| = 2.7264$ m, $H_z = 0.129$ m, the azimuth axis tilt angles $\psi_t = 1.854°$ and $\psi_a = 236.06°$, the dual-axis non-orthogonal angle $\tau_1 = 5°$, and the canting angle μ is roughly $-(1 - 5/60)° = -0.92°$. $\psi_t = 1.854°$ and $\psi_a = 236.06°$ were indirectly measured with the CMM using least squares fit of some points on the table plane of the heliostat model, orthogonal to the azimuth axis. $\tau_1 = 5°$ is the design value for the dual-axis non-orthogonal angle, verified with an angle gauge with the minimum increment of 5′. The canting angle μ of the heliostat model was designed as 1°, but the metal bar connecting the altitude motor shaft with the flat glass mirror was known to be slightly distorted before the laser beam

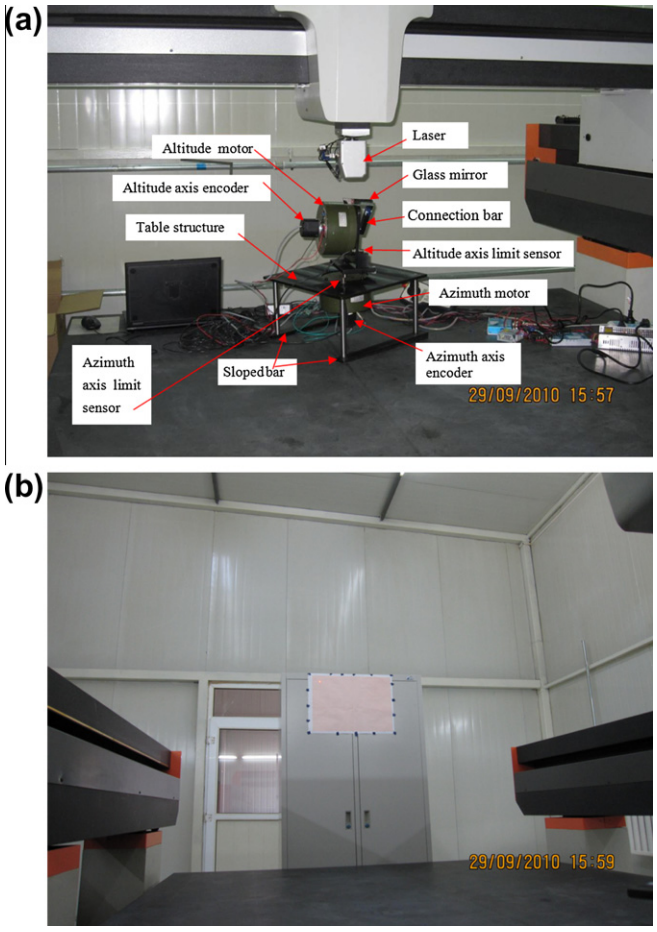

Fig. 4. Altitude–azimuth laser beam tracking test setup for a special designed heliostat model on a CMM platform. (a) geometry of the heliostat model and laser, (b) size and position of the target plane.

tracking test. The angle gauge was used to measure the angle between the bar edge and the front end plane of the altitude motor for μ, instead of the angle between the mirror plane and the altitude axis. The measurement scale had 5′ divisions, so the accuracy was $(5/60)^\circ = 0.08^\circ$. Due to the narrow measuring space, the angle gauge could not fit the motor front end and the connecting bar well, so the measured value of -0.92° for μ may be inaccurate.

4.2. Laser beam altitude–azimuth tracking test

For a real heliostat, the sun moves while and the target is fixed when the heliostat tracks the sun. The laser beam tracking test set-up had a fixed laser beam vector, while the mirror centre reflection vector could be changed within a reasonable range.

Two sets of laser beam tracking tests were done to verify the general altitude–azimuth tracking angle formulas for a heliostat with a mirror pivot offset and other fixed geometrical errors. The first set of heliostat model tracking tests conducted on September 29, 2010 included nine altitude–azimuth tracking tests with the nine reflected laser beam points nearly uniformly distributed on the target plane. Another set of 25 laser beam tracking tests were done on September 30, 2010, with the 25 reflected laser beam points randomly distributed on the target plane. Considering the limited encoder resolution and that the input tracking angles to the two motor controllers were in 0.1° increments, each tracking test first moved both motors to the desired angular positions and then the laser beam was moved to the marked mirror surface center, with the position of the reflection of the laser beam on the target plane, then noted. The data for the nine laser beam tracking tests on September 29, 2010, is reported in Table 1. The U–V locations of the nine laser beam reflection points in the tracking tests listed in Table 1 are plotted in Fig. 5. The data for the 25 laser beam tracking tests on September 30, 2010, is reported in Table 2. The U–V locations of the 25 laser beam reflection points for the random tracking tests listed in Table 2 are plotted in Fig. 6. The points in Figs. 5 and 6 show the positions of the laser beam reflection ever having landed at specific points on the target plane with the numbering indicating the measurement order. Both sets of the laser beam reflection points fill nearly the entire range of the target plane.

These two sets of laser beam tracking tests were also used to verify the validity of the least squares model and the effectiveness of Hartley-Meyer solution algorithm.

4.3. Determination of the angular parameters of the heliostat mode from tracking test data

As the 3rd rows in both Tables 3 and 4 show, the parameters $\psi_t = 1.854^\circ$, $\psi_a = 236.06^\circ$, $\tau_1 = 5^\circ$ and $\mu = -0.92^\circ$ were used as the nominal angular parameters for the heliostat mode, with the values of $\gamma_0$and α_0 unknown before the least squares solution. Although $\mu = -0.92^\circ$ was only approximated, it was still accurate enough for the nominal value of μ. These nominal values of the four angular parameters are good references to evaluate the accuracy of the numerically determined parameters.

4.3.1. Case one

The data in Table 1 was analyzed using the least squares model and the Hartley-Meyer solution algorithm to deter-

Table 1
First set of laser beam altitude–azimuth tracking test data with $\|\mathbf{OT}_0\| = 2.7264$ m.

Test order	1	2	3	4	5	6	7	8	9
Recorded altitude angle α_i' (°)	76	76.1	76.3	75.2	73.5	73.4	73.3	74.9	75.1
Recorded azimuth angle γ_i' (°)	−58.1	−53.5	−49	−49.2	−49.5	−54	−58.5	−58.3	−53.7
U of laser beam reflection (mm)	46	251	447	449	448.5	251.5	50	47	251
V of laser beam reflection (mm)	38	46	37	140	297	293	288	141	140

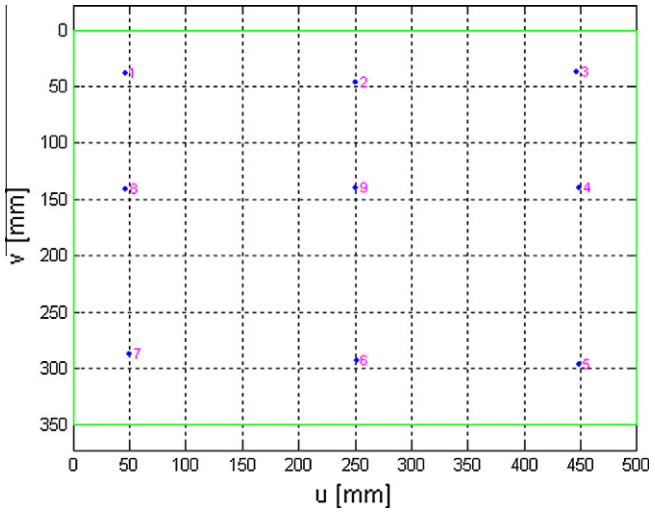

Fig. 5. Reflection points of the laser beam on the U–V target plane for the nine points in the first set of altitude–azimuth tracking tests.

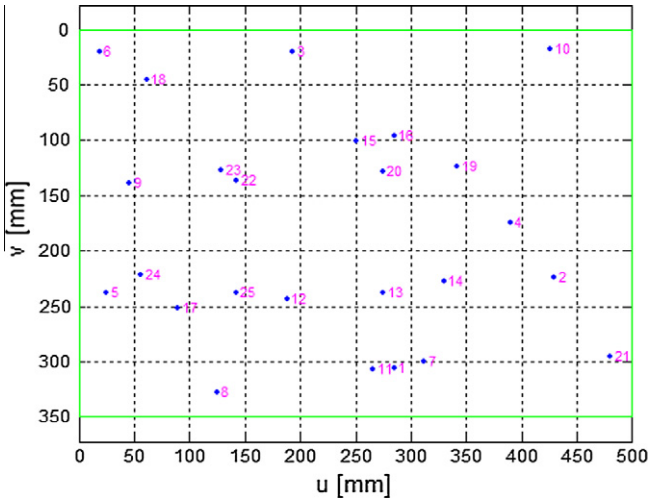

Fig. 6. Reflection points of the laser beam on the U–V target plane for the 25 points in the second set of altitude–azimuth tracking tests.

Table 2
Second set of laser beam altitude–azimuth tracking test data with $\|\mathbf{OT}_0\| = 2.7264$ m.

Test order	α'_i (°)	γ'_i (°)	u'_i (mm)	v'_i (mm)
1	73.3	−53.3	284	307
2	74.3	−49.8	431	222
3	76.3	−54.7	199	23
4	74.8	−50.6	392.5	174
5	73.8	−59.0	26.5	241
6	76.2	−58.7	20	17
7	73.4	−52.6	314	297
8	72.9	−56.9	126	332
9	74.9	−58.3	48.5	141
10	76.5	−49.4	430	20
11	73.3	−53.7	266	304
12	73.9	−55.3	191	242
13	74.0	−53.3	279	241
14	74.2	−52.1	331	227
15	75.5	−53.6	253	101
16	75.6	−52.8	288	94
17	73.7	−57.6	90	255
18	75.9	−57.8	63	48
19	75.3	−51.6	343	126
20	75.2	−53.1	277	130
21	73.5	−48.8	480	299
22	75.0	−56.1	146	139
23	75.1	−56.4	131.5	130
24	74.0	−58.2	62	225
25	73.9	−56.3	146	240

mine the six angular tracking parameters for the heliostat model given in the 2nd row in Table 3 with $\varepsilon_1 = 10^{-6}$, $\varepsilon_2 = 10^{-6}$ and $\beta_b = 10^{-5}$. The initial values $(\psi_a^0, \psi_t^0, \gamma_0^0, \tau_1^0, \alpha_0^0, \mu^0)$ for the Hartley-Meyer algorithm are given in the 1st row in Table 3. The regression gave $\vec{x}^* = (\psi_a, \psi_t, \gamma_0, \tau_1, \alpha_0, \mu) = (235.6524°, 1.9192°, 122.9386°, 5.3865°, 22.8152°, -0.4186°)$. The sum of the squares of the nine error functions in Eqs. (19) and (21) was $S(\vec{x}^*) = 10.4443$ mm^2, and the root of mean square of the error functions in Eq. (35) was $rms\_error(\vec{x}^*) = 1.0773$ mm.

Table 3
Initial and final values for the six angular tracking parameters for the first set of tracking tests.

Angular parameters	ψ_a (°)	ψ_t (°)	γ_0 (°)	τ_1 (°)	α_0 (°)	μ (°)
Initial values	−50	0.1	−250	0.1	1.0	−0.1
Regression results	235.6524	1.9192	122.9386	5.3865	22.8152	−0.4186
Nominal values	236.06	1.854	Unknown	5	Unknown	−0.92

Table 4
Initial and final values for the six angular tracking parameters for the second set of tracking tests.

Angular parameters	ψ_a (°)	ψ_t (°)	γ_0 (°)	τ_1 (°)	α_0 (°)	μ (°)
Initial values	235	1	−1	5	1.0	−0.3
Regression results	234.5745	2.0114	123.1650	5.4232	22.7568	−0.2615
Nominal values	236.06	1.854	Unknown	5	Unknown	−0.92

Relative to $\|\mathbf{OT}_0\| = 2.7264$ m, 1.0773 mm is about 0.4 mrad which is quite small compared to $0.1° = 1.7$ mrad.

4.3.2. Case two

Analysis of the data in Table 2 gave the six angular tracking parameters listed in the 2nd row in Table 4 with $\varepsilon_1 = 10^{-6}$, $\varepsilon_2 = 10^{-6}$ and $\beta_b = 10^{-5}$. The initial values $(\psi_a^0, \psi_t^0, \gamma_0^0, \tau_1^0, \alpha_0^0, \mu^0)$ for the Hartley-Meyer algorithm are given in the 1st row in Table 4. The regression gave $\vec{x}^* = (\psi_a, \psi_t, \gamma_0, \tau_1, \alpha_0, \mu) = (234.5745°, 2.0114°, 123.1650°, 5.4232°, 22.7568°, -0.2615°)$. The sum of the squares of the 25 error functions was $S(\vec{x}^*) = 34.2726$ mm^2, while the root of mean square of the error functions was $rms\_error(\vec{x}^*) =$

1.1709 mm. Relative to $\|\mathbf{OT}_0\| = 2.7264$ m, 1.1709 mm is about 0.43 mrad, again quite small compared to $0.1^\circ = 1.7$ mrad.

5. Discussion

The regression angular parameters (ψ_a, ψ_t, γ_0, τ_1, α_0, μ) from the two cases for the same laser beam altitude–azimuth tracking heliostat model, are slightly different, which is not unusual with multiple regression analyses. One set of tracking tests to determine the six angular parameters represent only one section of the multivariate sample space in probability theory. In addition, the system has additional unidentified error sources that are not included in the least squares model. Random error sources can result in noise in the measurements and the laser-beam tracking tests could be influenced by human and environmental factors. The laser beam reflection on the target plane sometimes wobbled, the target paper was not perfectly flat, the front cabinet wall could not be perfectly flat and vertical, and one person had to stand and move on the CMM platform during the laser-beam tracking tests to closely identify the centre of the beam on the target plane. There could also be some systematic distance errors in the laser beam tracking geometry. Hence, the regression angular parameters will depend a small amount on the specific experimental data. The agreement of the two sets of regression angular parameters is limited by the experimental conditions and the test system accuracy.

Although the two sets of calculated angular parameters differ, both sets are acceptable based on their RMS errors on the target plane. The RMS errors are quite small and close to 1 mm. Thus, both sets parameters are acceptable and within the limits of the system.

Either set of the calculated angular tracking parameters can be used in the general altitude–azimuth tracking formulas given by Guo et al. (2011) for the heliostat model. Use of the angular parameters from Case One with the second set of tracking test data gives a *rms_error* of 2.1630 mm, while using the angular parameters from Case Two with the first set of tracking test data gives a *rms_error* of 2.1503 mm. These two examples using the calculated angular parameters show that the average *rms_error* is about 2 mm; thus, the least squares technique given here is effective and both tracking parameter sets can be used for normal laser beam altitude–azimuth tracking of the heliostat model.

Both sets of calculated angular parameters differ from the six nominal angular tracking parameters listed in Table 3. Since there was no knowledge of γ_0 and α_0 before the laser beam tracking tests, only the nominal values for ψ_t, ψ_a, τ_1 and μ can be used to check the reasonableness of the least squares estimates. The comparisons in Tables 3 and 4 show that both sets of estimated angular parameters are reasonable.

The exact values for the six angular parameters for a real heliostat in the field are unknown, or may not be known, so accurate tracking parameters must be determined in the field. Hence, either set of angular values is preferable to the nominal values. In fact, the nominal values lead to a larger RMS error compared to the calculated angular parameters for both sets of experimental data. Field calibration of the tracking parameters will also compensate for unknown systematic errors in a heliostat.

This least squares technique has good convergence and numerical stability. Many sets of initial values of (ψ_a, ψ_t, γ_0, τ_1, α_0, μ) were tried in the least squares analysis and the iterating process always converged to the same values for the six angular parameters. Thus, the calculated angular parameters based on specific experimental data are insensitive to the initial values. $(\psi_a^0, \psi_t^0, \gamma_0^0, \tau_1^0, \alpha_0^0, \mu^0) = (-50^\circ, 0.1^\circ, -250^\circ, 0.1^\circ, 1.0^\circ, -0.1^\circ)$ and $(\psi_a^0, \psi_t^0, \gamma_0^0, \tau_1^0, \alpha_0^0, \mu^0) = (235^\circ, 1^\circ, -1^\circ, 5^\circ, 1.0^\circ, -0.3^\circ)$ are just two typical sets of initial values used for the two cases.

6. Conclusions

General, accurate altitude–azimuth tracking angle formulas have been developed for a heliostat with a mirror-pivot offset and other fixed geometrical errors. This paper presents a least squares model and an efficient solution algorithm (Hartley-Meyer algorithm) to determine the six unknown angular tracking parameters in the extensional altitude–azimuth tracking formulas. These angular parameters are the tilt angle, ψ_t, and the tilt azimuth angle, ψ_a, of the azimuth axis, the dual-axis non-orthogonal angle, τ_1, the canting angle, μ, of the mirror surface plane relative to the altitude axis, the angular bias, α_0, of the zero angle position of the altitude axis, and the angular bias, γ_0, of the zero angle position of the azimuth axis.

A specially designed heliostat model constructed on a 3D CMM platform with laser beam altitude–azimuth tracking was then used to verify this least squares model and the Hartley-Meyer solution algorithm. Data from two sets of laser altitude–azimuth tracking tests were used to calculate the six angular parameters for the heliostat model. The experimental tracking test data yielded two slight different sets of angular parameters from the least squares regression. Although the calculated angular parameters were dependent on the specific set of tracking data, the RMS tracking errors for each set were very small, indicating that both sets of angular parameters can be used. Hence, the least squares model and the Hartley-Meyer solution algorithm provided in this paper are quite useful for determining the angular parameters for the typical laser tracking heliostat model.

Further work will focus on the effectiveness of the least squares model and the Hartley-Meyer solution algorithm on real heliostats in Beijing 1 MW solar tower plant.

Acknowledgements

This work was supported by the National Natural Science Foundation of China (51006096) and the National Basic Research Program of China (2010CB227104).

References

Berenguel, M., Rubio, F.R., et al., 2004. An artificial vision-based control system for automatic heliostat positioning offset correction in a central receiver solar power plant. Solar Energy 76 (5), 563–575.

Guo, M.H., Wang, Z.F., et al., 2010. Tracking formulas and strategies for a receiver oriented dual-axis tracking toroidal heliostat. Solar Energy 84 (6), 939–947.

Guo, M.H., Wang, Z.F., et al., 2011. Accurate altitude–azimuth tracking angle formulas for a heliostat with mirror-pivot offset and other fixed geometrical errors. Solar Energy 85 (5), 1091–1100.

Jones, S.A., Stone, K.W., 1999. Analysis of strategies to improve heliostat tracking at Solar Two. Tech. Rep. SAND99-0092C, Sandia National Laboratories, Albuquerque, New Mexico.

King, D.L., 1982. Beam Quality and Tracking Accuracy Evaluation of Second Generation and Barstow Production Heliostats. SAND82-0181, Sandia National Laboratories, Albuquerque, New Mexico.

Lipps, F.W., Vant-Hull, L.L., 1978. A cellwise method for solar central receivers systems. Solar Energy 20, 505–516.

Mavis, C.L., 1988. 10 MWe Solar Thermal Central Receiver Pilot Plant Heliostat and Beam Characterization System Evaluation. Report SAND87-8003, Sandia Laboratories, Albuquerque, New Mexico.

Strachan, J.W., 1993. Revisiting the BCS, a measurement system for characterizing the optics of solar collectors. In: 39th International Instrumentation Symposium, Albuquerque, New Mexico.

Stone, K.W., Jones, S.A., 1999. Analysis of Solar Two Heliostat Tracking Error Sources. Tech. Rep. SAND99-0239c, Sandia National Laboratories, Albuquerque, New Mexico.

Zhang, G.C., Huang, S.Y., et al., 1989. Optimum Calculating Methods (in Chinese). Chengdu University of Science and Technology Press, Chengdu, ISBN 7-5616-0355-X, pp. 113–125.